

ANALYSIS AND APPLICATIONS OF A GENERALIZED MULTI-FIELD TWO FLUID APPROACH FOR PLUNGING JET CONFIGURATION

E. Krepper¹, F. Zidouni², D. Lucas¹

¹Helmholtz-Zentrum Dresden-Rossendorf (HZDR) Institute of Fluid Dynamics
P.O. Box 510119, D-01314 Dresden, Germany
E.Krepper@hzdr.de; D.Lucas@hzdr.de

²Theoretical and Applied Fluid Mechanics Laboratory, Faculty of Physics – USTHB,
P. O. Box 32 El Alia Bab Ezzouar 16111 Algiers, Algeria
zidounifaiza@yahoo.fr

ABSTRACT

The paper describes the simulation of a plunging jet. A generalized approach developed for the simulation of two-phase flow problems with multi-scale interfacial structures is applied for this problem. The GEneralized TwO Phase flow (GENTOP) modeling approach considers different scales in term of interfacial structure. The explicit statistical simulation of the interface between continuous gas and fluid is combined with the Euler/Euler simulation of dispersed gas. For the dispersed gas the Multiple Size Group (MUSIG) approach simulates different bubble sizes. The mass transfer between the bubble sizes is considered by bubble breakup and coalescence models. The gas entrainment during the plunging jet is described by the transition between continuous gas and dispersed gas. Here for a special sub grid model is applied.

This set of models is applied for the simulation of plunging jet experiments performed by Chanson et al. (2004). In the tests different geometric scale of plunging jet were investigated and here analyzed. The paper shows the capabilities of this approach and identifies weak points which need further development.

KEYWORDS

CFD, two phase flow, Euler/Euler approach, interfacial area, plunging jet

1 INTRODUCTION

Plunging jets into a large water reservoir play a role at lots of industrial applications. An essential phenomenon of a plunging jet into a large water reservoir is the entrainment of air. The entrained air has a strong influence on the flow field below the jet and on the mixing behavior. Dependent on the applications the entrained air might be desirable, in others not. The description of this phenomenon and determination of the entrained gas play an important role. The simulation of this complex process requires the consideration of different flow morphologies.

Recently a generalized approach developed for the simulation of two-phase flow problems with multi-scale interfacial structures (GENTOP) was developed and the applicability of this model concept to different flow situations was shown (Hänsch et al. 2012). The GENTOP modeling approach considers different scales in term of interfacial structure. The Multiple Size Group (MUSIG) approach (Frank et al.,

2008) considers different bubble size classes of dispersed gaseous flow. The GENTOP concept extends MUSIG the by the additional consideration of continuous gas. The interfacial momentum transfer for the continuous gas and liquid for area density and drag are applied according the local morphology of the gas phase in the same manner like the Algebraic Interfacial Area Density (AIAD) model. The AIAD model considers the shear stresses occurring at a free surface and was widely tested for the simulation of horizontal flow (Höhne & Mehlhoop, 2014). The explicit simulation of the interface between continuous gas and fluid is combined with the Euler/Euler simulation of dispersed gas. For the simulation of the air entrainment at the plunging jet phenomenon the transition between continuous gas and dispersed gas is described by a sub grid model of entrainment air source at the impinging region developed by (Ma et al., 2011). The transition between the different bubble sizes of dispersed gas is simulated by adequate bubble coalescence and breakup models.

Within this set of models, three geometric scale of plunging jet according to experiments performed by Chanson et al. (2004) were investigated (see Tab. 1). Those experiments have a same free jet length over jet diameter ratio ($h/d = 4$) where a detailed air–water measurements (void fraction, bubble count rate, bubble sizes) were presented for identical inflow Froude numbers can be found.

2 COMPUTATIONAL MODELING

2.1 The GENTOP concept

The Generalized Two Phase flow (GENTOP) -concept is based on a three-field two-fluid simulation. The flow is represented by a continuous liquid phase l , a polydispersed gas phase dg and a continuous gas phase cg . The small-scale dispersed gas is modelled in the framework of the inhomogeneous Multiple Size Group (MUSIG) -approach to deal with different bubble size groups and associated velocity fields (Frank et al. 2008). Within the polydispersed gas phases, transfers between different bubble size groups due to coalescence- and breakup are taken into account by appropriate models. Obviously more polydispersed phases with own velocity fields can be added in the framework of the inhomogeneous MUSIG-model.

The gaseous dispersed phase is divided into N velocity groups (gas phases), each characterized by its own velocity field. This enables to describe very roughly the dependency of the momentum exchange on the bubble size. For some components of non-drag forces this dependency has a great influence on the flow regime (Tomiyama, 1998; Lucas et al., 2007). The overall bubble size distribution is further represented by dividing the bubble diameter range within each of the velocity groups j into a number, $M_j(j=1,\dots,N)$, bubble sub-size fractions (see Fig. 1). The setup of bubble size fractions has to be a compromise between exact description of the flow and computational effort.

In the actual paper the inhomogeneous MUSIG approach is extended by mass transfer models from continuous gas into the dispersed gas respective vice versa dependent on the flow situation (see Fig. 1). They are based on a sub grid model proposed by Ma et al. (2011) (see. chapter 2.3). The exchange between the size fractions of the dispersed phase is organized according to the specified bubble breakup and coalescence models.

A proper cell size has to be chosen depending on the simulated bubble size distribution and the size of gas structures for which the gas–liquid interface has to be resolved.

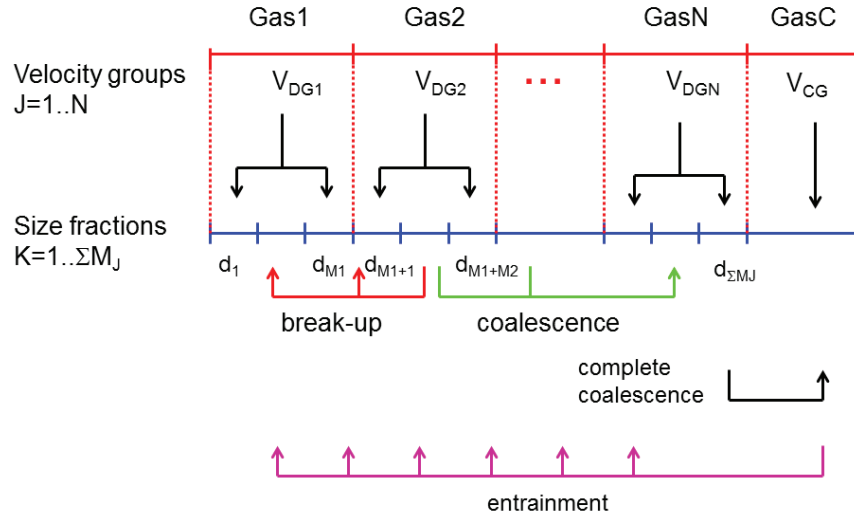


Fig. 1: Schema of the GENTOP model applied for impinging jet with gas entrainment

2.1.1 Free surface detection

The gas-liquid interface is detected using local information of the volume fractions via a function φ_{fs} . Due to the averaged treatment of the Euler-Euler approach, the expected volume fraction discontinuity at the interface, has been replaced by a gradient of volume fraction. A free surface region is defined using the volume fraction gradient of the continuous gas $|\nabla\alpha_{cg}|$ instead of the volume fraction.

The interface between the gas and the liquid is characterized by a variation of the volume fraction of $\nabla\alpha_{cg}$ from 0 to 1 over a number of n grid cells of a Δx size, which leads to a critical value $|\nabla\alpha_{cg}|_{crit} = 1/(n \Delta x)$ that allows a definition of the interface.

The free surface function is defined as:

$$\varphi_{fs} = 0.5 \tanh\left[a_{fs} \Delta x \left(|\nabla\alpha_{cg}| - |\nabla\alpha_{cg}|_{crit} \right)\right] + 0.5 \quad (1)$$

For the constants $n=4$ and $a_{fs}=100$ resulted in a reasonable shape of the interface.

2.1.2 Clustering Force

Considering the transitions from the dispersed to the continuous gas a situation might occur where the volume fraction of the continuous gas is much smaller than 1, which violates any physical sense. This malfunction was tried to solve by a so called ‘‘clustering force’’, which has an effect of collecting the scattered gas fractions. It is defined as

$$M_l^{clust} = -M_{cg}^{clust} = -c_{clust} (1 - \varphi_{fs}) \varphi_{clust} \rho_l \nabla\alpha_l \quad (2)$$

ρ_l is the liquid density and $\nabla\alpha_l$ the gradient of the liquid volume fraction. c_{clust} was set to 1.

where
$$\varphi_{clust} = (0.5 \tanh[a_B (\alpha_{cg} - \alpha_{clust, \min})] + 0.5) \cdot (0.5 \tanh[a_B (\alpha_{clust, \max} - \alpha_{cg})] + 0.5) \quad (3)$$

2.1.3 Complete coalescence

At some flow conditions, a simultaneous presence of the small bubbles and continuous gas within the same computational cells can occur. To prevent this artificial unphysical phenomenon, an additional coalescence model for complete gaseous mass transfer has been established. In this case the mass transfer is defined as:

$$\dot{m}_{dg \rightarrow cg} = (1 - \varphi_{fs}) \varphi_{morph} \rho_{dg} \alpha_{dg} \frac{1}{\tau_{dg \rightarrow cg}} \quad (4)$$

$\tau_{dg \rightarrow cg}$ is a time scale of the reaction and should be in the order of one time step of the transient calculation.

$$\tau_{dg \rightarrow cg} = 1 * \Delta t \quad (5)$$

The function φ_{morph} describes the region of the complete coalescence and was here defined as

$$\varphi_{morph} = 0.5 \tanh[a_B(\alpha_{cg} - \alpha_{cg,crit})] + 0.5 \quad (6)$$

For $\alpha_{cg,crit}$ a value of 0.3 was set, based on the knowledge that bubbly flow rarely exceeds a void fraction between 0.25 and 0.35 then changes into resolved structures (Griffith, P., 1961, Toombes et al., 2007).

The mechanism is turned off within the free surface region, so that mass transfers between different gas phases are possible from and to the filtered interface of the continuous gas. More details of the concept can be found in (Hänsch, S. et al. 2012).

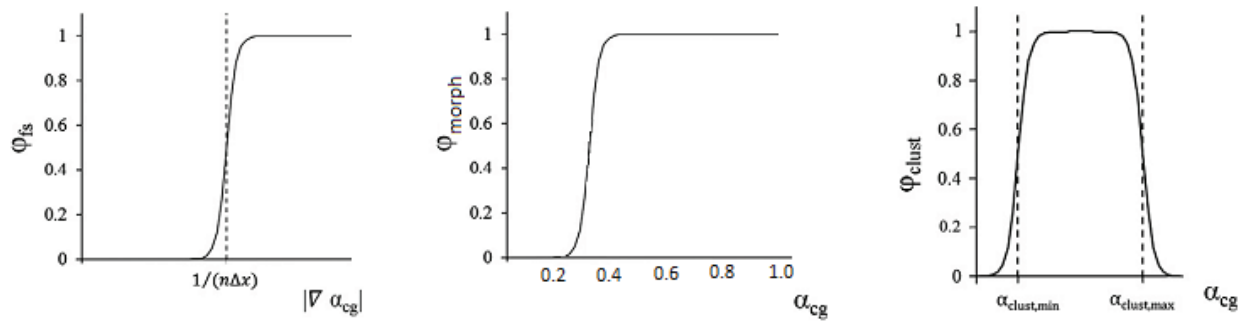


Fig. 2: Blending functions used within the GENTOP process

2.2 Modelling of the free surface drag

Interfacial transfer models for area density and drag are applied according to the local morphology of the gas phase via the free surface detection function.

For the drag between the continuous gas and the liquid the AIAD closure models of (Höhne T. et al., 2014) are applied for the continuous gas taking into account shear stresses τ_w and the slip velocity u_{slip} occurring at the surface as shown in equations (7) and (8). These closure models were successful tested for horizontal flow situations.

$$A_{D, fs} = \left(2|\nabla\alpha_l||\nabla\alpha_{cg}| \right) / \left(|\nabla\alpha_l| + |\nabla\alpha_{cg}| \right) \quad (7)$$

$$C_{D, fs} = \max \left(0.01, \frac{2[\alpha_l \tau_{w,l} + \alpha_{cg} \tau_{w,cg}]}{\rho_l u_{slip}^2} \right) \quad (8)$$

2.3 Sub-grid model for air entrainment

(Ma, J. et al., 2011) proposed a sub grid model deriving from a simple argument that the turbulent kinetic energy near the liquid-gas interface causes the interface to develop air cavities. These cavities are drawn into the liquid, see figure 3. Therefore the entrainment rate could be simply proportional to the downward gradient of the downward liquid velocity on the free surface and the local turbulent kinetic energy of the liquid as shown in equation (9) and (10).

$$Q_g(x) = \frac{q_g(x)}{\varphi_{fs}} = \frac{C_{ent}}{g \varphi_{fs}} k(x) \frac{\partial u_n}{\partial n}(x) \quad (9)$$

$$\text{where the normal vector } \vec{n} = \frac{\vec{\nabla}\alpha_l}{|\vec{\nabla}\alpha_l|} \text{ and } u_n = \vec{u} \cdot \vec{n} \quad (10)$$

C_{ent} is a constant depending on the fluid properties. In the calculations a value of $C_{ent} = 0.02$ was used.

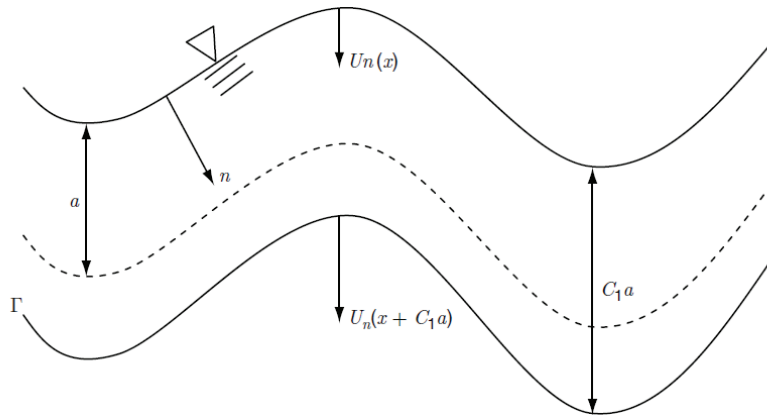


Fig. 3: Schematic diagram of air entrainment process at liquid-gas interface (Ma, J. et al., 2011)

3 VALIDATION EXPERIMENTS

The simulations presented in this paper, have been validated using an experimental database of Chanson et al. (2004). The section below the geometric, flow condition and measured parameters are detailed.

The experiments are performed with three scale models (M1, M2 and M3) that have the same Froude number and similar ratio $h/d=4$. The three tests were performed with different water quality with the consequence of a different surface tension, different nozzle diameter and different inlet velocity. In the

tests air fraction, bubble rate and bubbles sizes were measured. The water jet was ejected vertically down from a nozzle of diameter, d , onto cylindrical vessel with a mean exit velocity, V_0 , plunging into a pool located at a distance h , from the nozzle, as shown in figures 4a and b.

Changing the experimental conditions, the results highlight that the modelling of plunging jet based upon a Froude similitude is affected by significant scale effects when the approach flow conditions satisfied $We < 1000$, while some lesser scale effect was noticed for $V_1 / u_r < 10$ and $We > 1000$. According these experiments results sensitivity upon inlet velocity V_0 the air entrainment coefficient is conducted in the present work.

Bubble chord time measurements showed pseudo-chord sizes of entrained bubbles ranging from less than 0.5 mm to more than 10 mm with an average pseudo-chord size were between 4 and 9 mm. Two bubble sizes distribution of different class size and group velocities are adopted in order to get a better representation of the simulated experiment. Such different distribution allows estimating its influence on the plume behavior and air entrainment flow rate.

Tab. 1: Test parameters

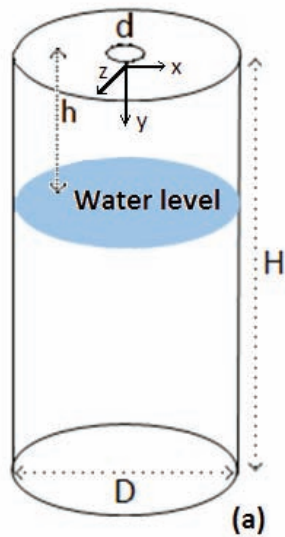
Parameters	M1	M2	M3
Surface Tension [N/m]	0.055	0.073	0.073
Vessel diameter [m]	0.1	0.05	0.0273
Vessel height [m]	0.75	0.5	0.45
Nozzle diameter [m]	0.025	0.0125	0.00683
Free jet length [m]	0.1	0.05	0.0273
Jet velocity [m/s]	4.1	3.04	2.16
Froude Number	7.2	7.1	7.1

4 SIMULATIONS

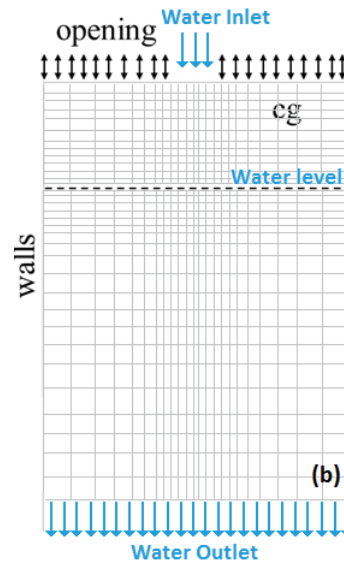
4.1 Modelling setup

The calculations were performed with the CFD code ANSYS-CFX. In all calculations presented in this section, the computational fluid domain includes the water bath, and the air above the water surface. The Cartesian coordinate system origin was placed on the inlet at the jet exit. The axial and transversal coordinates are y (downward) and x & z , respectively. The entire computational domain is represented by non-uniform three-dimensional spatial grids, adequately refined in the near-jet axis and water free surface.

All boundary conditions used to describe the flow field are reported in Figure 4. A liquid mass flow outlet equal to the entering mass flow was chosen in order to avoid a rise of water level inside the domain. At the walls free slip conditions for the fluids were applied. The upper section of the domain is modelled as an opening boundary condition with a relative pressure of 0Pa. The initial flow conditions are set for the water level. The free surface is applied with an initially smeared free surface region.



(a) Cylindrical tank filled of water through a nozzle above the free surface



(b) Axial Cross section and schematic grid representation and boundaries

Fig. 4: Geometry, fluid domain and boundary conditions

Beside the liquid phase three gas phases are simulated: The first two Gas1 and Gas2 as polydispersed gas phases in the framework of the inhomogeneous MUSIG approach and the third GasC as continuous gas. The momentum exchange between polydispersed gas and liquid by drag, lift, turbulent dispersion and virtual mass was defined according to the in the HZDR defined baseline approach for bubbly flow (Rzehak et al. 2013a). Bubble induced turbulence was considered (Rzehak et al. 2013b). The polydispersed gas phases are defined consisting of 7 bubble size classes as shown in Figure 1. The bubble size groups ranging from $d_{MIN}=1.5$ mm to $d_{MAX}=7.5$ mm. The two poly-dispersed gas phases are introduced to consider the different velocity fields for small and large bubbles caused by the change of the sign of the lateral lift force. According to Tomiyama et al. (2002) this critical bubble diameter is at about 6 mm for air-water flows at ambient conditions. Bubbles smaller than 6 mm (groups 1 to 5) are assigned to the first gas phase while bubbles between 6 and 8 mm (groups 6 and 7) belong to the second gas phase. Earlier investigations have shown that the bubble size distribution has a sensitive influence on the shape of the plume (Zidouni et al. 2011). All gas structures larger than an equivalent spherical bubble diameter of 8 mm are represented by the continuous gas phase GasC.

The interfacial transfer models applied for the different fluid pairs are summarized in Table 2. Mass transfer processes among the bubble size classes are described by using the model of Prince and Blanch (1990) for coalescence and the model of Luo and Svendsen (1996) for breakup. The ratio of breakup and coalescence coefficient F_B/F_C used is 0.5 and 1.0.

Furthermore the models between the continuous gas and liquid are applied as described in Section 2. The $k-\omega$ SST turbulence model is used for the liquid phase, together with the separated phase model for the drag coefficient and no turbulence modeling for the air phase (indicating a laminar flow).

Tab. 2: Bubble size classes, velocity groups and their corresponding applied models for interfacial transfers								
	Gas1 (G1..G5), Gas2 (G6, G7)							GasC
Morphology	polydispersed							continuous
Bubble classes	G1	G2	G3	G4	G5	G6	G7	
D_i [mm]	1.5	2.5	3.5	4.5	5.5	6.5	7.5	≥ 8
Drag	Ishii Zuber							Eq (8)
Lift force	Tomiya							None
Turbulent Dispersion	Favre Averaged							None
Bubble induced turbulence	Sato							None

The simulations are performed with the drag formulation in equation 8. The entrainment coefficient C_{ent} was set to 0.02.

4.2 Numerical setup

For transient time integration the fully implicit second order backward Euler scheme was used. For each time step, order of 0.0005 s, convergence had to be achieved within 5 to 35 coefficient loops using the averaged residual convergence criteria of $RMS=1e-04$. The simulations were run until the solution reached a quasi-steady state verified by a constant gas air entrainment. The time averaged of all parameter are presented in the following sections

5 RESULTS AND DISCUSSION

5.1 Time evolution of the volume fraction contours

The time evolution of air the entrainment, Figure 5, shows a realistic and physical plunging jet behavior considering the entire process of impingement, penetration and the rise of the gas structure to the free surface. The air cavity, the free surface motion can also be captured. As the deeper part the cavity breaks, it forms a continuous gas structure. This structure disappears progressively due to the break-up hence a small bubbles plume is created around the jet axis that developed deeper in the water tank. As the steady state is reached the air cavity is contracted within a small region of the impinging jet and no more large structure below the free surface is obtained.

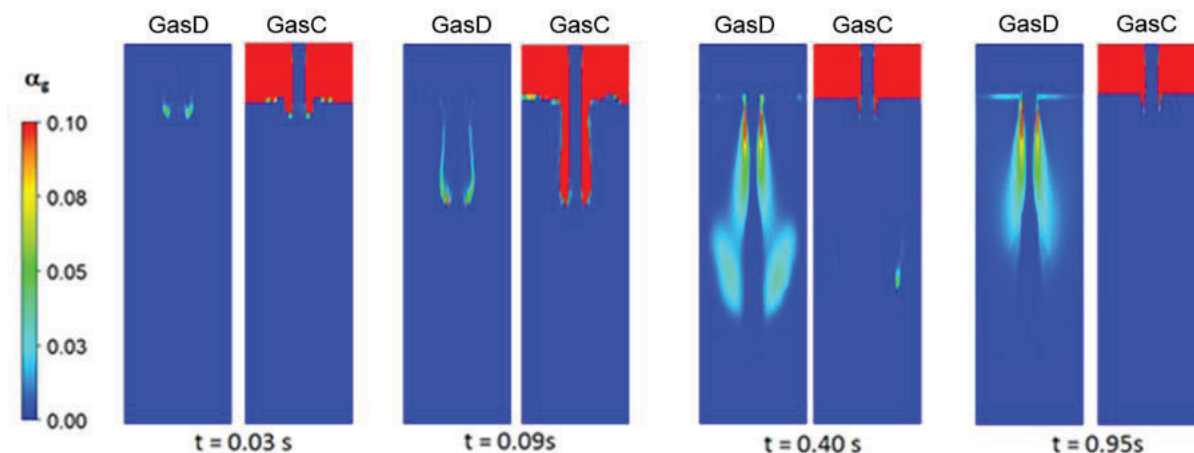


Fig. 5. Volume fraction distribution of dispersed gas (GasDisp) and continuous gas (GasCont) at three different times for the test case M2

5.2 Comparison of different tests

As already described in chapter 3 the tests were performed for three different arrangements of nozzle diameter, jet length and of water quality. The latter has consequences for the surface tension. At different scaled depth below the jet impingement plane $Y=1.6, 2.5$ and 4.1 the gas void fraction profiles were measured. Figure 6 shows the comparison to the calculations. The scaled depths were determined by

$$Y_i = \frac{y_i - h}{D_j} \quad (11)$$

with the spatial coordinate y_i , the jet length h and the jet diameter D_j . The profiles are shown for a problem time when the transient solution has reached steady state conditions. At this phase of the transient the continuous gas below the water surface already disappeared and the profiles show the distribution of dispersed gas.

The tests were performed for different plunging velocities. Unfortunately only for one velocity per arrangement the profiles were presented in the paper of Chanson et al. (2004). The comparison given in Figure 6 shows an excellent agreement for the tests M1 and M2 but weak reproduction for the test M3.

6 SUMMARY AND CONCLUSIONS

The simulation demonstrates the application of a concept modelling two phase flow regimes with both Euler/Eulerian approach of dispersed gas and the explicit simulation of large gaseous structures. The simulations showed that the model structure enables to capture the main flow characteristics of the entrainment phenomena. An accurate reproduction of the motion near the impinging region and the subsequent creation of the small bubbles plume around the jet axis were obtained. Furthermore a good agreement of the air entrainment rate and air volume fraction profile is obtained for most of the test cases.

It should be stated, that the main goal of the paper is to demonstrate the capability of the modelling concept. Some sub models are very preliminary and need further improvement.

The interfacial surface between continuous gas and liquid here expressed by eq. (1) need a careful consideration since its size has a sensitive influence on the entrainment calculated by eq. (9, 10). The mechanisms “clustering force” and “complete coalescence” (chapters 2.1.2, 2.1.3) in their actual formulation fulfill their purpose but improvements towards a more physical formulation are possible.

The bubble size distribution of arising dispersed gas during the plunging jet gas entrainment can be considered, the real distribution for the actual test however is unknown. In the actual simulations a guess was used. In the actual simulations bubble breakup and bubble coalescence were considered but the improvement of the models is still an issue. Previous work has shown that the bubble size distribution has strong influence on the shape of the plume.

Different model constants have to be determined analyzing more different tests under different flow conditions. During the next steps the model has to be applied to more experiments to show whether the approach is able to reproduce the main flow tendencies.

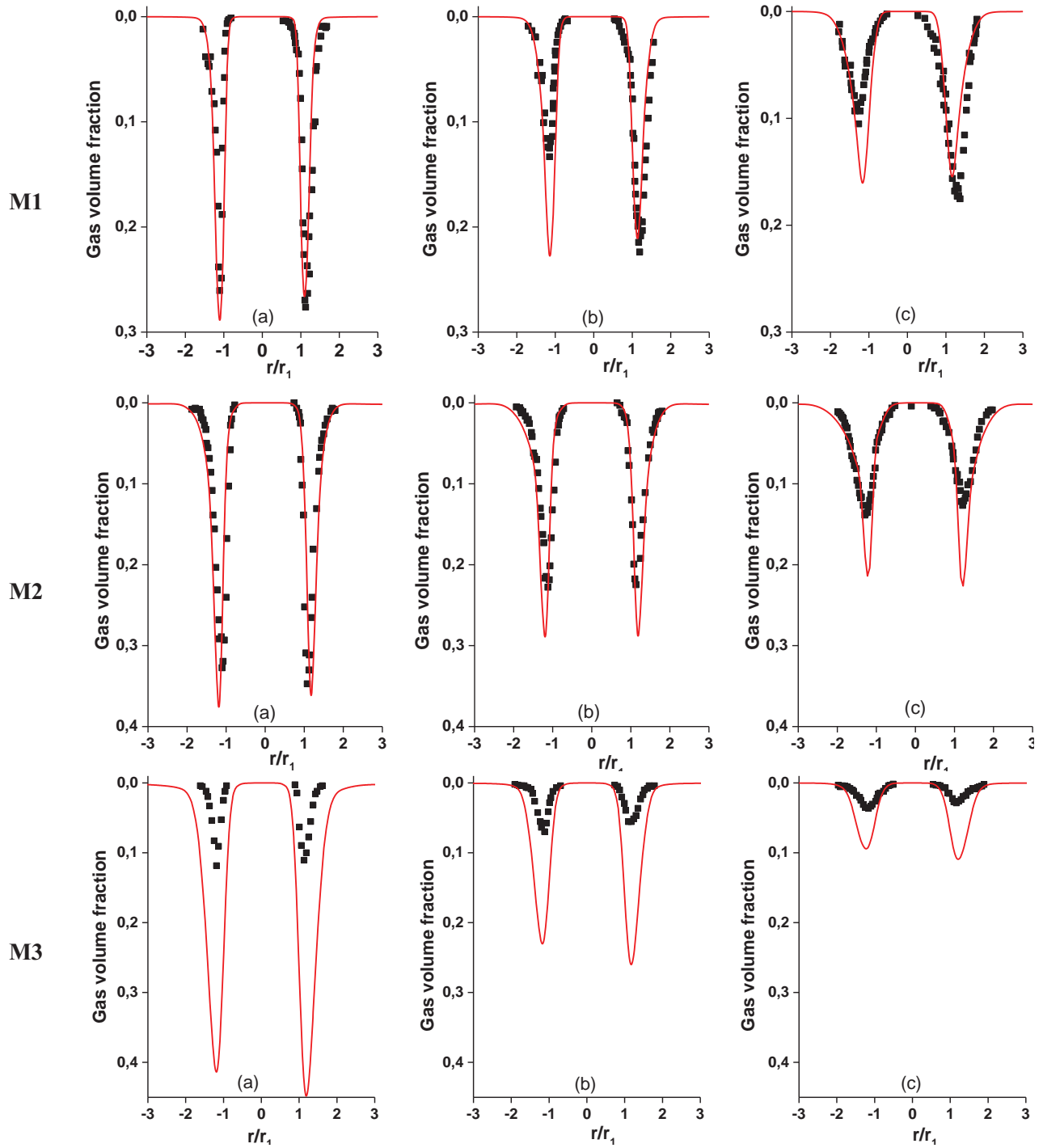


Fig. 6. Measured (points) and calculated (solid lines) Air volume fraction profiles for three geometric scales in the chanson experiment at different depth positions: (a): $Y_1=1.6$, (b): $Y_2=2.5$ and (c): $Y_3=4.1$

7 NOMENCLATURE

Notation	Unit	Denomination
α_{dg}	-	volume fraction of the dispersed gas Gas1 + Gas2
α_{cg}	-	volume fraction of the continuous gas GasC
α_l	-	volume fraction of the liquid
φ_{fs}	-	[0..1] presence of the interfacial area
φ_{clust}	-	[0..1] region of active cluster force
φ_{morph}	-	[0..1] description of morphology. Used for the calculation of the drag coefficient and the area of complete coalescence
M^{clust}	[N m ⁻³]	cluster force
$C_{D,fs}$	-	drag coefficient in the interface
$A_{D,fs}$	[m ⁻¹]	interfacial area density
$\tau_{W,l}$	[N m ⁻²]	liquid shear stress
$\tau_{W,cg}$	[N m ⁻²]	gas shear stress

8 REFERENCES

1. Chanson H., Aoki S., Hoque A., (2004) Physical modeling and similitude of air bubble entrainment at vertical circular plunging jets, *Chemical Engineering Science* 59 747 – 758
2. Frank, T.; Zwart, P.; Krepper, E.; Prasser, H.-M. & Lucas, D. 2008. Validation of CFD models for mono- and polydisperse air–water two-phase flows in pipes, *Nuclear Engineering and Design*, 238, 647-659
3. Griffith, P.; Wallis, G.B. (1961) Two-phase slug flow. *J. Heat Transfer* 83: 304-320 (1961).
4. Haensch, S.; Lucas, D.; Krepper, E. & Höhne, T. (2012) A multi-field two-fluid concept for transitions between different scales of interfacial structures, *International Journal of Multiphase Flow*, 47, 171–182
5. Höhne, T. & Mehlhoop, J.-P. (2014) Validation of closure models for interfacial drag and turbulence in numerical simulations of horizontal stratified gas-liquid flows, *International Journal of Multiphase Flow*, 62, 1 – 16
6. Iguchi, M., Okita, K. (1998) Mean Velocity and Turbulence Characteristics of Water Flow in the Bubble Dispersion Region Induced by Plunging Water Jet, *International Journal of Multiphase Flow*, 24, 4, pp. 523-537
7. Luo, H. & Svendsen, H. F. (1996) Theoretical Model for Drop and bubble-Breakup in Turbulent Dispersions. *AIChE Journal*, 42, 1225-1233
8. Ma, J.; Oberai, A.; Drew, D.; Lahey Jr., R. & M.C., H. (2011) A comprehensive sub-grid air entrainment model for RANS modeling of free-surface bubbly flows, *The Journal of Computational Multiphase Flows*, 3, 41-56
9. Prince, M. J. & Blanch, H. W. (1990) Bubble Coalescence and Break-Up in Air-Sparged Bubble-Columns. *AIChE Journal*, 36, 1485-1499
10. Rzehak, R.; Liao, Y.; Lucas, D. & Krepper, E. (2013a) Baseline Model for CFD of Dispersed Bubbly Flow. NURETH15-315
11. Rzehak, R. & Krepper, E. (2013b) CFD modeling of bubble-induced turbulence. *International Journal of Multiphase Flow*, 55, 138–155
12. Tomiyama, A. H. Tamai, I. Zun, S. Hosokawa, “Transverse migration of single bubbles in simple shear flows”, *Chem. Eng. Sci.*, **57**, 1849-1858, (2002).
13. Toombes L., Chanson H., “Surface waves and roughness in self-aerated supercritical flow”, *Environ Fluid Mech*, Vol. 7, 2007, pp. 259–270.
14. Zidouni Kendil, F.; Krepper, E.; Bousbia Salah, A.; Lucas, D.; Mataoui, A. (2011), “Numerical study of a bubble plume generated by bubble entrainment from an impinging jet”, *Nuclear Engineering and Design* 241, 4111-4121